ITER LIDAR performance analysis[a)]

M. N. A. Beurskens,[1,b)] L. Giudicotti,[2] M. Kempenaars,[1] R. Scannell,[1] and M. J. Walsh[1]
[1]*EURATOM/UKAEA Fusion Association, Culham Science Centre, Abingdon, Oxon OX14 3DB, United Kingdom*
[2]*Consorzio RFX—Associazione Euratom-Enea, Padova 35127, Italy*

(Presented 13 May 2008; received 12 May 2008; accepted 21 July 2008; published online 31 October 2008)

The core LIDAR Thomson scattering for ITER is specified for core profile measurements with a spatial resolution of 7 cm ($a/30$) for the range of 500 eV$<T_e<$40 keV and $n_e>3\times10^{19}$ m^{-3} at an accuracy of $<$10% for T_e. These specifications are verified using a full profile Monte Carlo simulation code. In the simulations it is assumed that the input transmission is 50% and the collection transmission is 10% for $\lambda=300-1200$ nm and $F/\#=6-17$. A crucial design decision lies on the choice of laser and detector combination. It is evaluated that the system can meet its spatial and accuracy specifications for higher temperatures of $T_e>5$ keV with a combination of a neodymium-doped yttrium aluminum garnet (Nd:YAG) laser ($\lambda_0=1064$ nm, $\Delta\lambda<1$ nm, 5 J, and $\Delta t_{\mathrm{FWHM}}=250$ ps, 5–10 Hz) and S20, GaAs, and GaAsP microchannel plate photomultipliers ($\Delta t_{\mathrm{FWHM}}<300$ ps, effective quantum efficiency, EQE=3%–4%, and $D=18$ mm). In order to reach the required T_e of 500 eV with Nd:YAG first harmonic, this choice requires a development of fast near infrared detectors. © *2008 American Institute of Physics.* [DOI: 10.1063/1.2969097]

I. INTRODUCTION

Simulation of the expected system performance of the ITER LIDAR diagnostic is crucial throughout the design phase of this system. This way the impact of variations in, e.g., the optical and/or laser design can be monitored. The target performance is given in Table I. In this paper a Monte Carlo code is discussed that will simulate the expected performance of the ITER LIDAR system in terms of the error in the measured electron temperature and density (T_e and n_e). In addition, profiles of T_e and n_e are calculated in order to visualize the expected performance. The code takes all relevant system variables into account such as, e.g., optical transmission, vignetting, laser performance, and detector response functions. In addition, the code has a simple user interface, an easy to use logging system, and a version control.

The basic design of the core LIDAR system is described in Refs. 1–5. An outline scheme for the collection optics is shown in Fig. 1. In the case shown, the laser beam is injected through a hole in the first light collection mirror. This has the key advantage of separating the requirements for high power handling of the laser mirror from a wide spectral bandwidth for the collection mirror at the expense of a small hole in the collection mirror. The scattered light is relayed through a labyrinth to the vacuum window at the rear of the port plug. The etendue for the Thomson scattered light in the system will be reduced with distance across the tokamak, with the minimum light collected at the inner wall. The system indicated in Fig. 1 has a variation of f-numbers from $\sim f/6$ at the outboard side to $\sim f/17$ at the inner wall. This is compatible with collecting the light scattered from the whole cross section of the laser beam onto a single detector with diameter typical of that of the available detectors (around 18 mm diameter at $f/0.7$).

Some examples of the scattered spectra[6] expected in ITER, including the substantial relativistic effects, are shown in Fig. 2. It is clear that at the highest temperature the spectrum is very broad and peaks significantly in the "blue" region. To get 40 keV at a scattering angle of 180° (LIDAR), one needs to measure down to $\lambda/\lambda_0\sim0.3-0.35$ (λ_0 is the laser wavelength). Typically, this extended region of the spectrum is problematic for high-optical transmission for both refractive and reflective components in the ITER environment due to the various effects of neutrons, gammas, and mirror degradation due to erosion or (mainly) deposition.

The current reference design of the ITER LIDAR system is based on a neodymium-doped yttrium aluminum garnet (Nd:YAG) laser running at its first harmonic of 1064 nm, 5 J laser energy, and 250 ps full width at half maximum (FWHM) pulse length (i.e., a compromise between power density and spatial resolution). Ideally, with a laser wavelength of 1064 nm, a wavelength range from 300 to 1200 nm is covered by the new system. Present relevant detectors are

TABLE I. System performance requirements.

Requirement	ITER LIDAR
Range	$r/a<0.9$
Temperature range	0.5–40 (keV)
Density range	3–30 (10^{19} m^{-3})
Resolution	7 cm ($a/30$)
Accuracy	10% in T_e and 5% in n_e
Repetition rate	100 Hz

[a)]Contributed paper, published as part of the Proceedings of the 17th Topical Conference on High-Temperature Plasma Diagnostics, Albuquerque, New Mexico, May 2008.
[b)]Tel.: +44-1235-464532. Electronic mail: marc.beurskens@jet.uk.

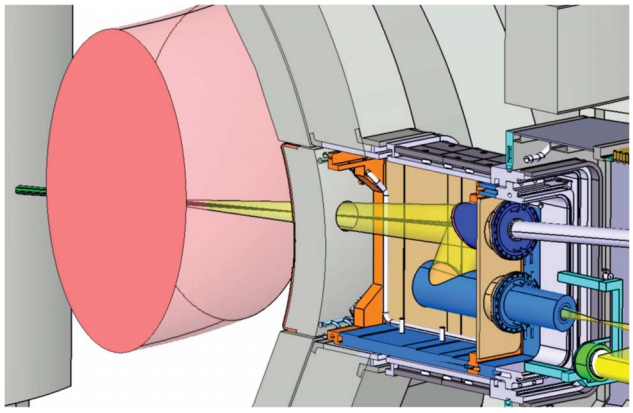

FIG. 1. (Color online) Conceptual design of input and collection optic.

microchannel plate photomultiplier (MCP-PMT), which are also used in the current JET LIDAR systems.[7,8] Available photocathodes are S20 (multialkali), gallium arsenide (GaAs), and gallium arsenide phosphate (GaAsP). The response of the complete system is set by a combination of the type of photocathode, the size of the detector, the detailed structure of the MCP-anode unit, and the electrical coupling. The three photocathodes considered cover the wavelength range from ~300 to ~850 nm. The S20 efficiently covers the range up to 480 nm. The GaAsP covers the next range up to approximately 750 nm with a relatively good sensitivity, and the GaAs covers the range from 500 to around 850 nm but with less sensitivity than the GaAsP. In order to meet the spatial resolution requirement of $a/30$, the detectors need to have a response time of around 350 ps FWHM. These speeds have been demonstrated with detectors with S20 and GaAsP cathode materials, albeit the detectors were smaller with a diameter of less than 11 mm. In order to cover the entire plasma cross section, a detector diameter of >18 mm is desirable, but the price to pay is that these larger cathode materials result in slower detectors partly due to their larger capacitance. The GaAs cathode needs to be thicker than the other two cathode materials, and as a consequence, MCP-PMTs with this cathode material tend to be slower even for the 11 mm sized detectors.[1]

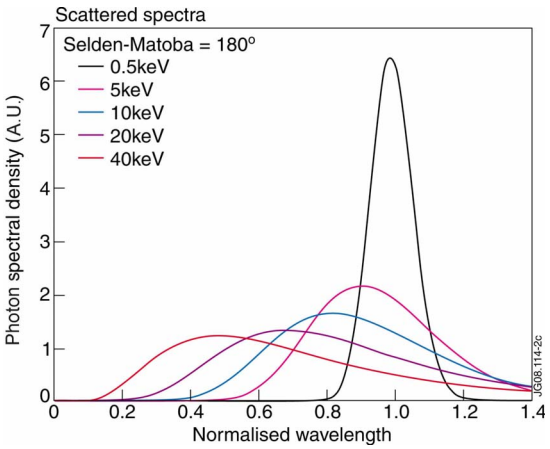

FIG. 2. (Color online) Theoretical Thomson scattering spectra for the required Te range in the ITER LIDAR system for the normalized laser wavelength.

TABLE II. Parameter description.

Parameter	Description
$R(t)$	Radius as a function of laser time of flight
$N_{\mathrm{pe},i}(R(t))$	No. of photoelectrons in channel i
T_l	Transmission of the laser input path
ΔL	Collection volume
$n_e(R(t))$	Electron density profile
$\partial\sigma/\partial\Omega$	Thomson scattering cross section
$\Delta\Omega(R(t))$	Solid angle of collection as a function of plasma radius
N_l	No. of laser photons proportional to laser energy E_l
$T_e(R(t))$	Temperature profile
$T_c(\lambda)$	Transmission of collection path as a function of wavelength
$\mathrm{EQE}_i(\lambda)$	Effective quantum efficiency
$\Phi_i(\lambda)$	Spectral filter characteristic
λ/λ_o	Wavelength normalized to incident laser wavelength

In order to meet the system performance requirements, MCP-cathode materials covering the wavelength range from 850 to 1200 nm are required to resolve lower temperatures of $T_e=0.5-5$ keV. Good candidate materials for this wavelength range are In–GaAs and InGaAs-TE (TE=transverse electron) cathode materials that show significant sensitivity in this area, but as a general rule they are not fast or sensitive enough. Reports of detectors with reasonable sensitivity in this area can be found elsewhere.[1] In this study we assume for some of the simulations that near infrared (NIR) detectors will be available at 2% and at 0.3% effective quantum efficiency (EQE=detector quantum efficiency/detector noise factor).

II. THOMSON SCATTERING FORMULAS AND PLASMA BACKGROUND LIGHT

In the simulation program, n spectral channels are introduced indexed with i. The spectral coverage for each of these channels i is defined by the filter characteristics $\Phi_i(\lambda)$. As LIDAR is a time of flight measurement, it is convenient to express the scattering formula in units of time, where the scattering volume is expressed as $\Delta L=\Delta t\cdot c/2$. The collected number of primary photoelectrons (pe) for spectral channel i would be

$$N_{\mathrm{pe},i}(R(t)) = \frac{c}{2}T_l N_l \frac{\partial\sigma}{\partial\Omega} n_e(R(t))\Delta\Omega(R(t)) \times \int_{\lambda=0}^{\lambda=\infty} S[T_e(R(t)),\lambda,\lambda_0,\theta] \times T_c(\lambda)\mathrm{EQE}_i(\lambda)\Phi_i(\lambda)\frac{\lambda}{\lambda_o}d\lambda \quad (1)$$

in units (pe/s) and in which $S[T_e(R(t)),\lambda,\lambda_0,\theta]$ is the relativistic scattering formula derived from Ref. 6. The other parameters are system parameters and are described in Table II.

The simulation code assumes bremsstrahlung as the plasma background light. The spectral line radiation from intrinsic impurities is not yet included and is envisaged for the later versions of the code. Instead, an enhancement factor

is included in the code in order to include additional background light level. The plasma bremsstrahlung is given by

$$\varepsilon(R,\lambda) = \frac{0.95 \times 10^{-19}}{\lambda 4\pi} g_{\mathrm{ff}} n_e^2(R) Z_{\mathrm{eff}}(R) T_e^{-1/2}(R) \times \exp\left[\frac{-hc}{\lambda T_e(R)}\right] \ (\mathrm{ph/sr\ m^3\ nm\ s}), \quad (2)$$

as derived from Ref. 9. The electron free-free Gaunt factor g_{ff} is taken as $g_{\mathrm{ff}}=0.6183\ \ln(T_e)-0.0821$. [At $T_e \gg 1$ eV, the exponent term in Eq. (2) approaches unity and the -0.0821 offset in g_{ff} becomes negligible]. The plasma background as seen by the detector i is the integral of Eq. (2) and requires inclusion of system parameters from Table II. As the etendue of collection is conserved, the plasma light as seen by the detector can be expressed as

$$\mathrm{PL}_D(\lambda,t) = \mathrm{EQE}_i(\lambda) T_c(\lambda) \Phi_i(\lambda) A_D \Delta\Omega_D \times \int_{R_{\mathrm{in}}}^{R_{\mathrm{out}}} \varepsilon(R,\lambda) dR \ (\mathrm{pe/nm\ s}), \quad (3)$$

where $A_D\Delta\Omega_D$ the detector's etendue, and R_{in} and R_{out} the radii of the inner and outer walls of ITER. On the time scale of the entire profile measurement of ~25 ns, this is assumed to be a constant level. In the simulated detector signals the plasma background therefore appears as a constant offset to the Thomson scattered signal [Eq. (1)].

III. SPATIAL RESOLUTION AND NUMBER OF PHOTONS IN THE SCATTERING VOLUME

In conventional imaging Thomson scattering systems the spatial resolution is the same as the scattering volume that determines the Poisson statistics. As LIDAR is a time of flight measurement, the spatial resolution of the system is determined by the temporal length of the laser pulse ($\Delta\tau_{\mathrm{laser}}$) and the response time of the detector ($\Delta\tau_{\mathrm{detector}}$). In principle, the digitizer bandwidth also plays a role, but modern digitizers and oscilloscopes have such high bandwidths (>4 GHz) that they do not need to be considered further ($\Delta\tau_{\mathrm{digitizer}} \ll \Delta\tau_{\mathrm{laser}}, \Delta\tau_{\mathrm{detector}}$). Assuming a Gaussian response for the laser and detector, the spatial resolution is determined by $\Delta L_{\mathrm{Resolution}} = (c/2)\sqrt{\Delta\tau_{\mathrm{laser}}^2 + \Delta\tau_{\mathrm{detector}}^2}$. However, the scattering volume that determines the photon statistics is given by the detector response time only, and hence $\Delta L_{\mathrm{detection}} = (c/2)\Delta\tau_{\mathrm{detector}}$. Ideally, in order to get the best signal to noise ratio for a given spatial resolution, a LIDAR system consists of a laser with a delta-function time response and only the detector response setting the spatial resolution. In practice, the laser response is dictated by the available laser technology and also by damage threshold power limits of optical laser components. A realistic time response for the laser therefore is ~250 ps. Hence, to meet the specification of spatial resolution a detector response of ~350 ps is required. Alternatively, both would have a response of ~300 ps.

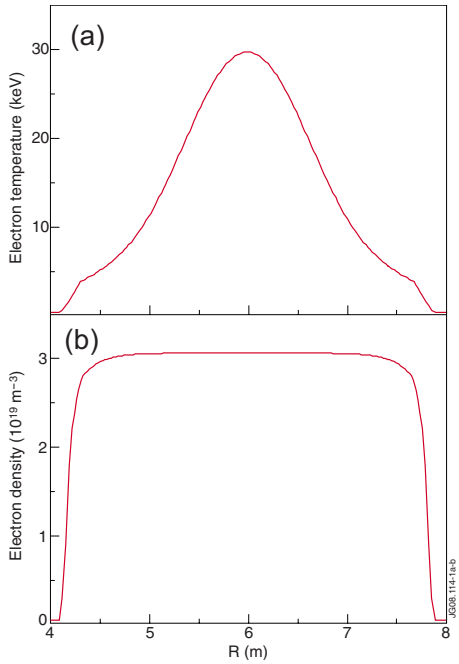

FIG. 3. (Color online) ITER T_e and n_e profiles used as input for the simulations. The profiles are for a typical ITER scenario at low density.

IV. SIMULATED THOMSON SCATTERING MEASUREMENTS

The signals as simulated in the code are derived from the assumed T_e, n_e, and Z_{eff} profiles. The T_e and n_e profiles used in this experiment are given in Fig. 3. These profiles are obtained from transport simulation for baseline ITER scenarios. The relativistic spectra for these temperatures are determined using formula (1) and the system parameters such as the solid angle (Fig. 4) and spectrometer characteristics (Fig. 5). The number of spectral channels and the number of channel transitions have been optimized using an optimization routine similar to that used in Ref. 10. In this example the laser energy was chosen to be 5 J, the system overall transmission was taken to be 50% of the laser input, and a flat 10% collection efficiency. The resulting Thomson scattering signals in all 7 channels of this example are given in Fig. 6(a). At this stage the signal has already been convolved with the laser pulse response (250 ps in this example). The

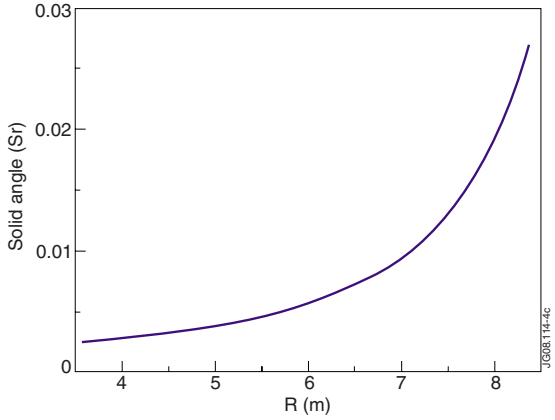

FIG. 4. (Color online) Solid angle of detection of ITER LIDAR design with a 36 cm diameter mirror.

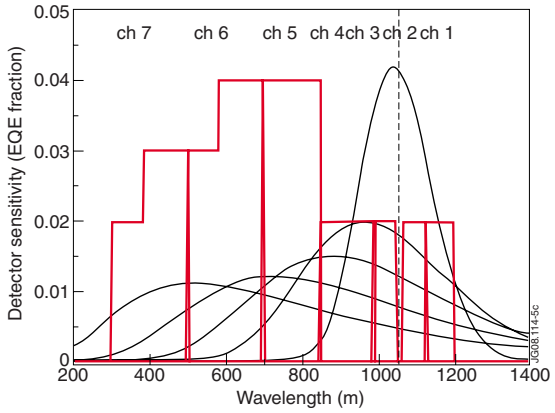

FIG. 5. (Color online) Example spectral layout as used in the simulation with the relativistic Thomson scattering spectra overlaid (0.5, 5, 10, 20, and 40 keV).

plasma background light has been added with an enhancement factor of 2 above the calculated bremsstrahlung level. The Poisson noise is then added for each of the digitizer bins (50 ps) and the signal is subsequently convolved with the detector response time, in this case, of 350 ps FWHM Gaussian, as is shown in Figs. 6(b) and 6(c).

Figure 7 shows the final result of the simulation. Figure 7(c) indicates that the statistical error for the entire profile is $<10\%$ for T_e and $<5\%$ for n_e. In this particular example, the

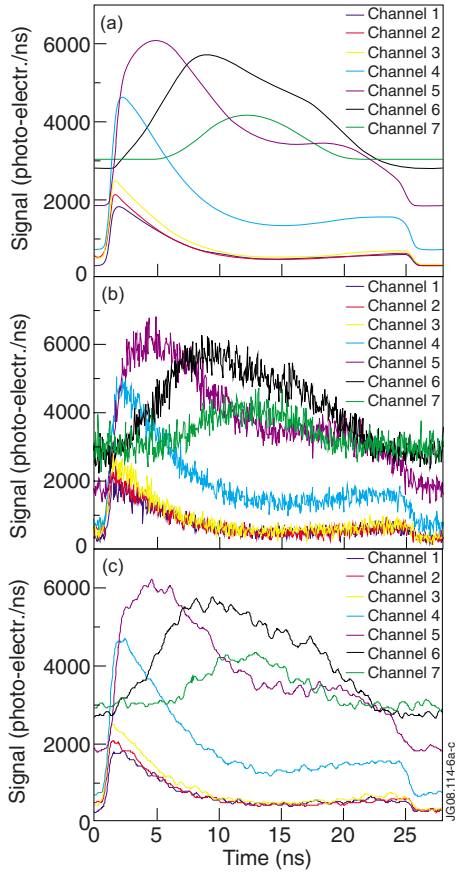

FIG. 6. (Color online) (a) Simulated Thomson scattering spectra and added plasma bremsstrahlung ($x2$) for the profiles in Fig. 4 and the seven channels in Fig. 5. (b) Poisson noise added to each of the digitizer bins (c) signal convolved with the detector instrument function.

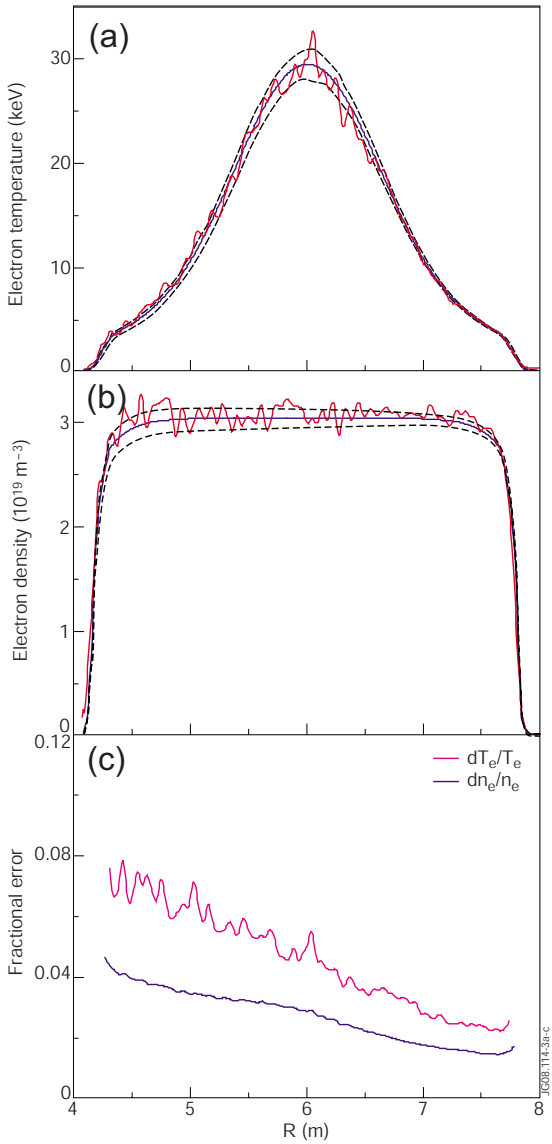

FIG. 7. (Color online) Profile fits (red) to the simulated signals for (a) electron temperature and (b) electron density. The black dotted lines indicate the 1-sigma error range. (c) Fractional errors as a function of radius. The increase in error inward is due to the decreasing solid angle of collection (Fig. 4).

system specification would be matched. It was assumed that NIR detector technology is available from 850 to 1200 nm with an EQE of 2%. These detectors do not exist yet. Therefore, simulations were also performed with NIR detectors at 0.3% and 0% EQE. Figure 8 gives an overview of all three cases for a point at $R=6$ m (center of the machine). It is immediately clear that the high temperatures >5 keV are not affected. This means that the profile in this example (Fig. 7) is still well covered in the range $R=4.5-7.5$ m. However, if lower temperatures need to be covered (as specified), new detector development is required.

V. FUTURE WORK

A Monte Carlo simulation code has been established that can monitor the impact of design decisions on the ITER LIDAR system performance. The current reference design based on a fundamental Nd:YAG has been tested. The laser

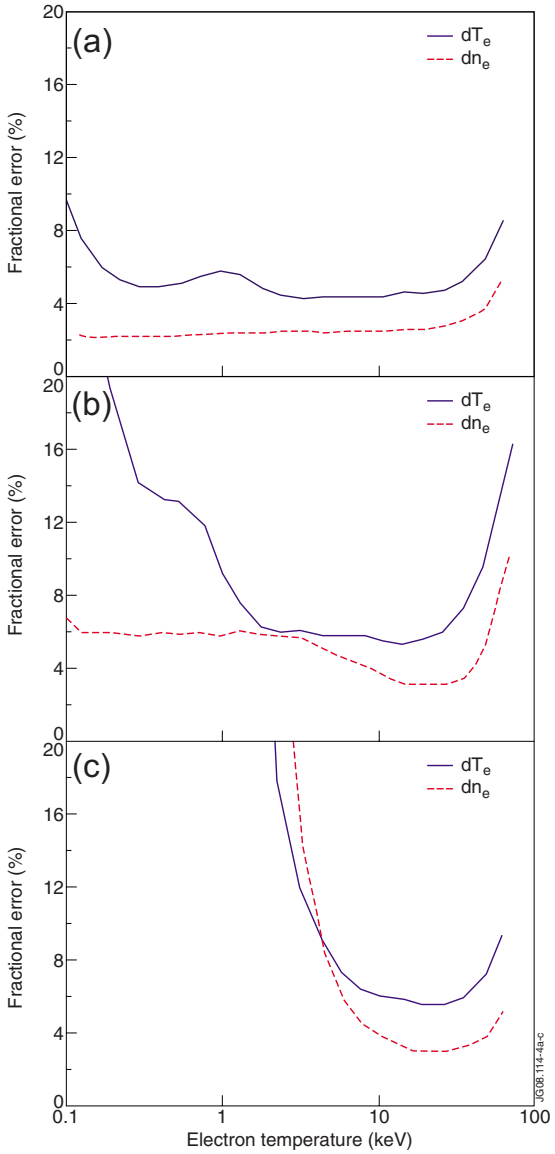

FIG. 8. (Color online) (a) Result from a Monte Carlo simulation using the spectrometer layout in Fig. 5. (b) With channels ch1–ch4 at 0.3% instead of 2% EQE and (c) without channels ch1–ch4.

energy and pulse duration were assumed to be 5 J and 250 ps FWHM, respectively. This laser technology is currently not commercially available at the required specification of 100 Hz. Multilaser solutions seem to be an attractive solution and would also give more flexibility of, e.g., running in burst mode (firing multiple lasers in rapid succession) and give redundancy in the system in case of breakdown. However, also lower rep-rate variants of the required laser are still under development. Detector technology has been assumed to include S20, GaAs, GaAsP cathodes, and NIR technology such as InGaAs and InGaAs-TE. MCP-PMTs with GaAsP cathodes are available that meet the full specification;[11] however, their diameter is ~11 mm. Larger detectors are available but they have slower response times. S20 detector technology is said (by the manufacturer) to also meet the requirements for detector with diameter of 10 mm at the given EQE assumed in this paper. Again larger detectors will be slower, but tests need to be carried out. Next, GaAs MCP-PMTs are available in the market with a sufficiently good sensitivity, but even the smaller models of 11 mm diameter are slower than the requested 350 ps FWHM. NIR technology with EQE=2% does not exist yet but the development is promising.

An alternative spectrometer design is under way that accommodates smaller detectors by splitting the system up into two parts covering respectively the low and the high field sides of the ITER plasma. The feasibility of such a system will be evaluated with the currently developed simulation code. Also alternative laser designs will be evaluated. The use of Ti:sapphire, for example, will not require NIR detectors as the laser will run at 800 nm. Another option of covering the low temperature gap could be the use of a second harmonic Nd:YAG laser.

[1] M. J. Walsh, M. Beurskens, P. G. Carolan, M. Gilbert, R. B. Huxford, M. Loughlin, A. W. Morris, V. Riccardo, C. I. Walker, and Y. Xue, Rev. Sci. Instrum. **77**, 10E525 (2006).
[2] A. E. Costley, Proceedings of the 12th International Symposium on Laser-Aided Plasma Diagnostics, Snowbird, 2005 (unpublished), Paper No. I-A.1.
[3] G. Razdobarin, M. Walsh, T. Hatae, E. E. Mukhin, K. Narihara, G. Vayakis, D. Johnson, T. Carlstrom, and ITPA Specialists Working Group on Thomson scattering, 21st IAEA Fusion Energy Conference, Chengdu, China, 2006 (unpublished).
[4] L. de Kock, Design description document, Thomson scattering (core) LIDAR, 1998, ITER Document No. G 55 DDD 3 97-12-05 W 0.5.
[5] P. Nielsen, Update to Core Lidar system for ITER-FEAT, May 2001, EFDA Contract No. 00/557.
[6] O. Naito, H. Yoshida, and T. Matoba, Phys. Fluids **5**, 4256 (1993).
[7] H. Salzmann, J. Bundgaard, A. Gadd, and C. Gowers, Rev. Sci. Instrum. **59**, 1451 (1988).
[8] M. Kempenaars, P. Nelsen, R. Pasqualitto, C. Gowers, and M. Beurskens, Rev. Sci. Instrum. **75**, 3894 (2004).
[9] M. E. Foord, Rev. Sci. Instrum. **53**, 1407 (1982).
[10] O. Naito, H. Yoshido, S. Kitamura, T. Sakuma, and Y. Onose, Rev. Sci. Instrum. **70**, 3780 (1999).
[11] M. Kempenaars, I. Balboa, M. Beurskens, J. C. Flanagan, L. Giudicotti, and M. J.Walsh, High Temperature Plasma Diagnostic conference, Albuquerque, NM, 2008 (unpublished).